Finite-element calculations of the antiprotonic helium atom including relativistic and QED corrections

Nils Elander and Evgeny Yarevsky*
Department of Physics, Stockholm University, Box 6730, S-11385 Stockholm, Sweden
(Received 10 March 1997)

A recently developed extension to a three-dimensional finite-element Schrödinger equation solver in the total angular momentum representation was used to calculate the energy-level spectrum and wave functions for antiprotonic helium system. The accuracy of the numerical method was analyzed. Relativistic and QED corrections to the energy levels were calculated in the main order. Excellent agreement was reached between relativistically corrected wavelengths and recent experimental data. Radiative transition probabilities and lifetimes were calculated and compared with other calculations as well as with experiment.
[S1050-2947(97)06109-X]

PACS number(s): 36.10.−k, 02.70.Dh

I. INTRODUCTION

The spectrum of the general three-body Hamiltonian is considerably more difficult to study than that of the corresponding two-body problem. Accurate experimental results were available earlier only for heliumlike systems where optical methods have made it possible to determine a large number of doubly as well as singly excited energy levels. It is only recently that other systems have been studied in such great detail that they can be used as comparative benchmarks for general theoretical three-body methods.

Exotic atoms, i.e., atoms including a massive negatively charged particle, have been studied for some time. The first few investigations were purely theoretical, dealing with their spectral and other properties comparing them to normal atoms [1–3]. The computational methods were based on the Born-Oppenheimer (BO) approximation.

The observation of delayed antiproton annihilation in liquid helium [4] in 1991 changed the situation drastically. Considerable attention has since been given to the antiprotonic helium system $\overline{p}\mathrm{He}^+$. Both isotope systems $\overline{p}^3\mathrm{He}^+$ and $\overline{p}^4\mathrm{He}^+$ were experimentally studied in detail [4–16]. Recently, high-precision measurements of transition wavelengths have been reported for both $\overline{p}^4\mathrm{He}^+$ [7,11,15,16] and $\overline{p}^3\mathrm{He}^+$ [12] systems.

The experimental methods were based on laser-induced transitions in the visible spectral region giving a relative accuracy of 4 ppm. This has created a challenge to theoretical few-body physics. The $\overline{p}\mathrm{He}^+$ system is in this sense becoming an additional benchmark for computational three-body theory. This theoretical work has, on the other hand, challenged and guided experiment to observe more wavelengths and decay rates, thus completing and extending our knowledge of the antiprotonic helium system.

Despite the vast experimental data concerning decay rates, the formation and collisional quenching of the antiprotonic helium, etc., so far most theoretical work has been devoted mainly to calculations of energy levels of $\overline{p}\mathrm{He}^+$ [17–23]. Only a few papers have partially dealt with Auger processes [6,21] or formation and quenching processes [19,24,25] in the system.

Early theoretical attempts used the Born-Oppenheimer approximation [2,3,17]. The uncertainty reached within the frame of this approximation is less than 10^{-6} a.u. [17,18]. Recently, more extensive work have included the use of a configuration-interaction method [19], an adiabatic approximation method [18,20], and a variational method [21].

While the current experimental accuracy of the measured transition wavelengths is around 4 ppm, we found that most prior theoretical results [17–21] disagree with experiment to about 1000 ppm. Since each of the above-mentioned methods most likely has been pushed to its limit, the remaining discrepancies are to be found in the basic assumptions and perhaps the approximations made in each respective theoretical approach.

We reported preliminary results that are closer to the current experimental data [23]. These results are supported by the recent theoretical work of Korobov [22] (see below), which agrees with experimental transition wavelengths within 40 ppm.

In this work we use a three-dimensional finite-element method (FEM). The FEM has been used successfully earlier in engineering calculations [26]. The implementation of the FEM in quantum mechanics is rather rare [27–36] in spite of its advantages. By combining a total angular momentum representation and FEM, we have been able to calculate energy levels of the $\overline{p}^4\mathrm{He}^+$ system. However, comparing them to presently available experimental data, we obtain disagreement up to 40 ppm. The main part of this difference is shown below to be due to relativistic effects. When calculated, the relativistic corrections produce excellent agreement between our theoretical and current experimental data.

Because most experimental results for transition wavelengths [7,11,15,16] and decay rates [8,11] are presented for the $\overline{p}^4\mathrm{He}^+$ isotope system, we shall here restrict our consideration to this system. Calculations of the $\overline{p}^3\mathrm{He}^+$ system are in progress.

*Permanent address: Laboratory of Complex Systems Theory, Institute for Physics, St. Petersburg University, St. Petersburg, Russia.

 © 1997 The American Physical Society

The paper is organized as follows. In Sec. II, we describe the formal theory and how the obtained equations are realized in a numerical treatment. In Sec. III, the main results concerning nonrelativistic energy levels are presented. In Sec. IV, relativistic and QED corrections to the energy levels are reported. In Sec. V, we present and analyze radiative decay times and Einstein coefficients. The paper is concluded with a short summary.

II. METHOD OF CALCULATIONS

The $\overline{p}\mathrm{He}^+$ system consists of three particles interacting via Coulomb forces. Here we will neglect nonradiative decay channels; therefore, the energy levels will be truly bound states. The total wave function Ψ^{JM} of the system with the angular momentum J and its projection M can be expanded in terms of Wigner D functions [37,38]:

$$^{\pm}\Psi^{JM}=\sum_{s=0,1}^{J}\frac{1}{\sqrt{2+2\delta_{s0}}}[D^{J}_{Ms}(\alpha,\beta,\gamma) \pm(-1)^{s}D^{J}_{M-s}(\alpha,\beta,\gamma)]^{\pm}\psi^{(Js)}(\mathbf{R}). \quad (1)$$

Here plus and minus signs refer to states with normal and anomalous spatial parity, respectively. The Euler angles α, β, and γ define a rotation of the body-fixed frame with respect to the laboratory-fixed one and $\mathbf{R}$ is a three-dimensional coordinate in the body-fixed frame. As the states of the anomalous spatial parity decay rapidly via Auger transitions [1,22], the only states of interest can be described as $^{+}\Psi^{JM}$. In the following, we thus consider only such states and omit the plus in the designation of the wave function.

There are a few different possible choices of the body-fixed coordinate $\mathbf{R}$. The usual one [17,18,22] is ''standard'' Jacobi coordinates. Here the first vector joins two heavy particles (helium and antiproton) and the second connects the electron and the center of mass of the $\overline{p}\mathrm{He}^{2+}$; see Fig. 1(a). The main reason for that choice is that it is possible to separate the electron motion for the case of infinite masses of the heavy particles. However, we have chosen another Jacobi coordinate system plotted in Fig. 1(b). Namely, let particles 1, 2, and 3 represent the antiproton, the electron, and the helium nucleus, respectively. Then x is the distance between particles 2 and 3 (i.e., electron and helium nucleus), y is the distance between particle 1 (antiproton) and the center of mass of particles 2 and 3, and ϕ is the angle between $\mathbf{x}$ and $\mathbf{y}$. In short, this choice is caused by a simpler structure of the wave function in these coordinates and will be explained in Sec. III.

After substituting expansion (1) into the Schrödinger equation and using an orthogonality relation for the D function [37] one can derive the system of equations [38]

$$-i\sqrt{1+\delta_{s1}}\frac{\lambda_{-}(J,s)}{2\mu_{1,23}y^2}\left(\frac{\partial}{\partial\phi}+(1-s)\cot\phi\right)\psi^{(Js-1)} +[-\Delta^{(s)}_{x}-\Delta^{(s)}_{y}+V^{Coul}(x,y,\phi)-E]\psi^{(Js)} -i\sqrt{1+\delta_{s0}}\frac{\lambda_{+}(J,s)}{2\mu_{1,23}y^2}\left(\frac{\partial}{\partial\phi}+(1+s)\cot\phi\right)\psi^{(Js+1)} =0, \quad s=0,\ldots,J, \quad (2)$$

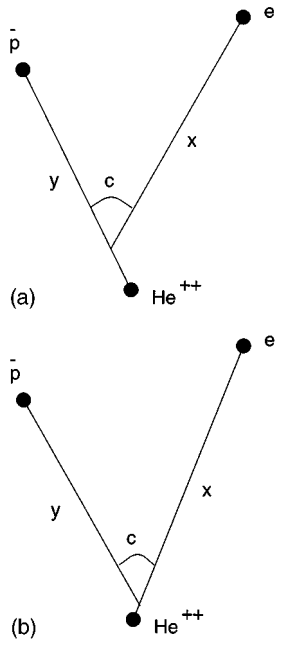

FIG. 1. Jacobi coordinate systems: (a) ''standard'' Jacobi coordinates and (b) our choice, discussed in the text. The angular variable $c=\cos\phi=(\hat{\mathbf{x}},\hat{\mathbf{y}})$.

where $\lambda_{\pm}(J,s)=[J(J+1)-s(s\pm1)]^{1/2}$ and $\psi^{(J-1)}\equiv0$. The diagonal part $-\Delta^{(s)}_{x,y}$ of the kinetic-energy operator and the Coulomb potential V^{Coul} are defined as

$$-\Delta^{(s)}_{x}=-\frac{1}{2\mu_{23}x^2}\left[x\frac{\partial^2}{\partial x^2}x+\left(\frac{\partial^2}{\partial\phi^2}+\cot\phi\frac{\partial}{\partial\phi}-\frac{s^2}{\sin^2\phi}\right)\right],$$

$$-\Delta^{(s)}_{y}=-\frac{1}{2\mu_{1,23}y^2}\left[y\frac{\partial^2}{\partial y^2}y-[J(J+1)-2s^2] +\left(\frac{\partial^2}{\partial\phi^2}+\cot\phi\frac{\partial}{\partial\phi}-\frac{s^2}{\sin^2\phi}\right)\right],$$

$$V^{Coul}(x,y,\phi)=-\frac{2}{r_{13}}-\frac{2}{r_{23}}+\frac{1}{r_{12}}.$$

The interparticle distances r_{ij} can easily be expressed in terms of Jacobi coordinates and the reduced masses μ have been defined in terms of the particle masses m_i as $\mu_{23}=m_2m_3/(m_2+m_3)$ and $\mu_{1,23}=m_1(m_2+m_3)/[m_1+(m_2+m_3)]$. The components $\psi^{(Js)}$ must satisfy the boundary conditions with respect to the angle ϕ so that

$$\psi^{(Js)}(x,y,\phi)=\sin^{s}\phi\,\tilde{\psi}^{(Js)}(x,y,\phi), \quad (3)$$

where $\tilde{\psi}^{(Js)}(x,y,\phi)$ is a bounded function of its arguments.

The most important advantage of the set of equations (2) is that they couple the three components $\psi^{(Js-1)}$, $\psi^{(Js)}$, and

$\psi^{(Js+1)}$ only. In a numerical realization this produces a band matrix with a fixed bandwidth for any angular momentum J. This decreases computational requirements substantially.

Numerically we have realized Eq. (2) using the finite-element method. Here we outline the general ideas of this method, while one can find its detailed description elsewhere [26,33,35].

The three-dimensional space formed by x, y, and $c=\cos\phi$ is divided into some number of rectangular boxes numbered by i. Each component $\tilde{\psi}^{(Js)}$ of the total wave function is expanded in a finite-element basis such that

$$\tilde{\psi}^{(Js)}(x,y,c)=\sum_{im} v_{im} f_{im}(x,y,c). \tag{4}$$

For the sake of simplicity, we omit the indices (Js) on the right-hand of Eq. (4). Here v_{im} are expansion coefficients defined in each element i and restricted through continuity conditions for the wave function at element boundaries. A basis function $f_{im}(x,y,c)$ has in the finite-element algorithm the property

$$f_{im}(x,y,c)\equiv 0 \quad \text{for } (x,y,c)\notin \text{element } i. \tag{5}$$

Then the coefficients v_{im} and the energy E are obtained by means of minimization of a functional $\langle\Psi|H|\Psi\rangle$, where the Hamiltonian H is defined in Eq. (2). The best approximation is evaluated by solving a generalized eigenvalue problem

$$\tilde{H}v=E\tilde{S}v,$$

where

$$(\tilde{H})_{im,jk}=\langle f_{im}|H|f_{jk}\rangle,$$

$$(\tilde{S})_{im,jk}=\langle f_{im}|f_{jk}\rangle. \tag{6}$$

It is worth noticing that the global basis set is a particular case of the method described above where one box only is used. However, the FEM manifests its advantages in using many boxes, defined by the locality of the basis functions (5). One such advantage is that the final matrices $\tilde{H}$ and $\tilde{S}$ become banded and relatively sparse and the overlap matrix $\tilde{S}$ is well defined in contradiction to the ill-defined one appearing for a global basis set.

Let us now discuss some details of the general scheme used for our calculations. The basis functions are expressed as products of one-dimensional basis functions

$$f_{im}(x,y,c)=f^{(x)}_{i,n(m)}(x)f^{(y)}_{i,k(m)}(y)f^{(c)}_{i,l(m)}(c). \tag{7}$$

Such a representation of the basis functions simplifies an evaluation of the matrix elements in Eq. (6) and reduces most three-dimensional integrals to a product of one-dimensional ones.

The number of boxes for the space coordinates x,y is defined by convergence properties. However, one box only was chosen for the angular variable c. The one-dimensional basis functions in every box were chosen to be

$$f^{(x)}_{i,n}(x)=P_n(\hat{x})\exp(-\nu x),$$

$$f^{(y)}_{i,k}(y)=P_k(\hat{y})g_d(y), \tag{8}$$

$$f^{(c)}_{i,l}(c)=P_l(c).$$

Here P_l is a Legendre polynomial and g_d is a damping function that will be discussed later. Variables $\hat{x}$ and $\hat{y}$ appear instead of x and y due to a normalization of every one-dimensional box to the interval $[-1,1]$. This normalization causes a maximum linear independence of the basis functions in the box and decreases the ill definiteness of the overlap matrix.

The above choice of the basis functions is guided by the fact that we are dealing with a Coulomb potential only. This makes it possible to use simple analytical expressions for the potential matrix element in Eq. (6) and to reduce the CPU time of the calculations as well as to increase the accuracy.

There are different possibilities in choosing a set of functions defined by Eq. (8). We have found that one of the most convenient set is the set with the bounded maximal power of polynomials

$$n+k+l\leqslant M. \tag{9}$$

In principle, one can use the functions defined by Eq. (8) with $\nu=0$ and $g_d(y)=1$. However, to speed up convergence, it is convenient to find an appropriate constant ν and a function g_d. We have fixed the damping function to meet the asymptotic behavior of the wave function at the origin and at infinity:

$$g_d(y)=Cy^J\exp\left(-\frac{\mu_{1,23}}{J+1+q}y\right). \tag{10}$$

Here q is an arbitrary parameter. Thus the only nonlinear parameters to be optimized are ν and q. We have found a slow eigenvalue dependence on these parameters. This enables the value of ν to be fixed $\nu=1.5$ for all levels and the value of q to be calculated on a small number of boxes.

Using this basis, the generalized eigenvalue problem (6) was solved by means of an inverse iteration procedure. For solving the set of linear equations so appearing, we used the block LU factorization method [39].

III. COULOMB ENERGY LEVELS

In this section we present our results for energy levels and transition wavelengths for the pure Coulomb case. The antiprotonic helium has properties that resemble both molecular and atomic systems. Both molecular rovibrational (v,J) and atomic (n,l) quantum numbers may be used in a level classification. The two sets of quantum numbers are related through [17]

$$n=v+J+1, \quad l=J. \tag{11}$$

In the following, we use the molecular classification scheme.

The mesh used in the calculations was fixed to meet the strong localization of the wave function [17,19]. The total number of elements was chosen to be 36. Six elements were used for x and y and only one element for c. This mesh is

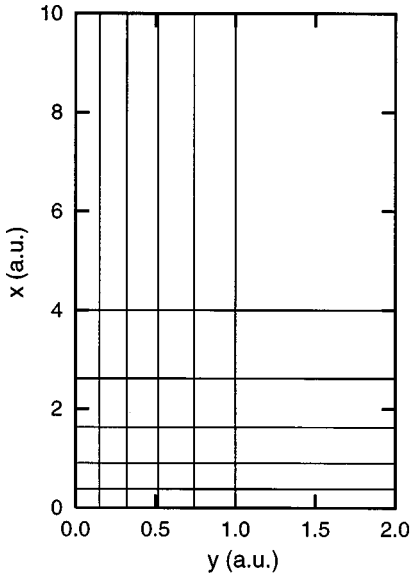

FIG. 2. Mesh used in calculations for x and y coordinates.

shown in Fig. 2. The matrix elements of the potential in Eq. (6) were calculated analytically with respect to c. Numerical integration for x and y was performed using the 30-point Gauss quadrature rule for the elements containing the Coulomb singularity and the 20-point one was used for the others. The number of functions for the c variable was fixed to be 19. An increase in the number of functions beyond 19 did not influence the results within the present accuracy.

The convergence properties of the numerical scheme has been proved as follows. The asymptotic behavior for an approximate eigenvalue $E^{(p)}$ can, for rather small element volumes h and large polynomial degrees p, be written as

$$E^{(p)}=E^{exact}+Ch^{2p}, \tag{12}$$

where C is some constant [26]. As our elements have very different volumes, we preferred to reach the final results by increasing p. When the asymptotic behavior (12) is reached, an estimate

$$\Delta(p)\equiv E^{(p+1)}-E^{(p)}=\widetilde{C}h^{2p} \tag{13}$$

is valid. One can see in Fig. 3 that the calculated results agree well with the theoretical prediction already in the range $p=3,\ldots,6$ both for polynomials only in Eq. (8) and for polynomials with the damping functions.

By means of extrapolation of the asymptotic behavior $E^{(p)}$ we can calculate E^{exact} and we can therefore estimate the error, which is equal to the difference between the extrapolated value E^{exact} and the calculated value $E^{(p)}$. We use the values calculated with the damping functions because of their higher accuracy. The accuracy defined in this way is 4×10^{-6} a.u. for $v=0,1,2$, 6×10^{-6} a.u. for $v=3$, and 15×10^{-6} a.u. for $v=4$.

The formalism, discussed above, yielded sparse matrices of dimension about 9000 with a total bandwidth of about 4000. All calculations were performed on a DEC/Alpha 600/4-256 workstation in double precision and took about 2 h of CPU time for each level.

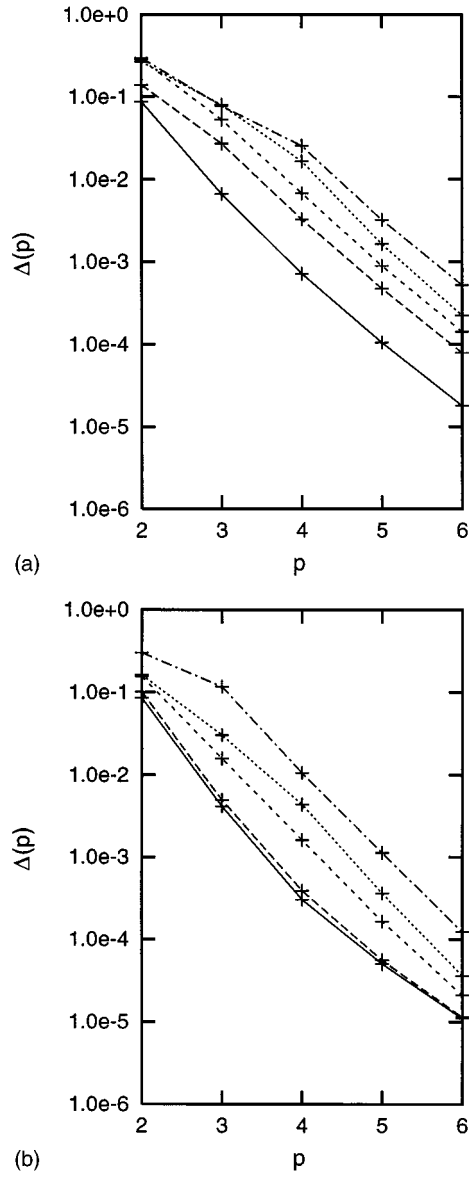

FIG. 3. Dependence of $\Delta(p)$ on the maximum degree of the polynomials p for $J=36$ and different vibration numbers v. The solid line, dashed line, short-dashed line, dotted line, and dash-dotted line correspond to $v=0,1,2,3,4$, respectively. The convergence for (a) only polynomials and (b) polynomials with the damping functions are shown.

Results for eigenvalues $E_{vJ}(N)$, converged within the present accuracy with respect to the number of equations N, are presented in Table I for a few typical values of (v,J). All energies are measured in atomic units. The masses of $^4He^{2+}$ and $\overline{p}$ adopted are $7294.299m_e$ and $1836.1527m_e$ [40].

One can see that the finite mass corrections as well as the corrections coming from higher equations have an essential influence on the final results. The corrections become larger for lower values of J. This is in accordance with the consideration of the validity of the BO approximation [17]. The difference between our and the BO results is inside the uncertainty of the BO approximation, which is of the order of the mass ratio $m_e/m_{\overline{p}}$. It can be seen that the main difference, especially for small values of J, comes from the higher

TABLE I. Energies (a.u.) of some levels of the $\overline{p}^4\mathrm{He}^+$ system. The results are presented for the BO approximation [18] and our calculations with one $[E(1)]$, two $[E(2)]$, and three $[E(3)]$ equations.

	Energies E_{vJ}				
(v,J)	BO	$E_{vJ}(1)$	$E_{vJ}(2)-E_{vJ}(1)$	$E_{vJ}(3)-E_{vJ}(2)$	Final
(1,39)	-2.610523	-2.610298	-0.000092	$< -1\times 10^{-9}$	-2.610391
(1,36)	-2.813061	-2.812883	-0.000219	-1.0×10^{-9}	-2.813102
(1,33)	-3.104987	-3.104909	-0.000461	-3.0×10^{-8}	-3.105370
(1,31)	-3.363874	-3.363901	-0.000739	-5.5×10^{-7}	-3.364640

equation corrections. As the functions $\psi^{(Js)}$ with $s\geqslant 1$ correspond to excited electron states, the energy-level shifts due to those states are of major importance in an exact calculation of the antiprotonic helium level structure.

We are now ready to explain our choice of the coordinate system used in Eq. (2). Although Eq. (2) becomes a BO approximation for infinitely heavy nuclei, the BO approximation does not give lower estimates for our energies as it usually does [18]. One can in Table I see that the $E(1)$ eigenvalues can be higher as well as lower than the BO eigenvalues. This is due to a change of the y coordinate when m_e/m_{He} was made nonzero.

However, there are two reasons for our choice of the coordinate system. The first reason is obvious from Fig. 4, where two cuts of the wave function for the typical level (0,36), obtained with our coordinate system and with the ''standard'' one, are displayed. One observes that the coordinate system that was used produces a much smoother variation than the standard one does. Thus, using our coordinate system, we can obtain a more accurate numerical wave function. Our choice is also guided by the fact that physically one may understand the system as a mainly spherical electron distribution around the helium nucleus, which is only slightly perturbed in the vicinity of the antiproton [17,19]. The second reason for our choice can be found by a comparison of Table I and Korobov's results [22] for the second equation correction [Korobov finds $E(1)=-2.812\,682$ a.u. and $E(2)-E(1)=-0.000\,432$ a.u. for the (1,36) level]. This correction is smaller in our coordinates and our choice of coordinates may thus also be important for calculations that include many equations. Studies of Auger rates is an example of such a case.

The corrections coming from the fourth equation of system (2) are very small. A typical additional energy-level shift does not exceed 10^{-7} a.u. Thus we have used only the first three equations in our calculations. However, we would like to mention that a larger number of equations is likely to be essential for an accurate description of antiprotonic helium with lower J values. In that case a description of the energy levels as truly bound states is incorrect since they are able to autoionize. It is then necessary to use some technique developed for resonant states, e.g., the complex rotation method [41].

Our basic results for the energy levels E_{vJ} and favored transition wavelengths

$$\lambda((v,J)\rightarrow(v,J-1))=[2R(E_{vJ}-E_{vJ-1})]^{-1} \qquad (14)$$

are presented in Tables II and III. For the Rydberg constant we used the value $R=10\,973\,731.5\ \mathrm{m}^{-1}$. Since our calculations are variational ones, the results given in Table II are upper estimates for the true energies.

Let us compare our results with recently published work of Korobov [22]. He used the same representation (1) of the total wave function Ψ^{JM}. To minimize the Hamiltonian he uses a global basis set expressed in spheroidal coordinates. The accuracy for most nonrelativistic energy levels was stated to be better than 10^{-7} a.u. We can see by a comparison of Table II herein and Table IV in Ref. [22] that our results agree within 10^{-5} a.u. for most energy levels. The

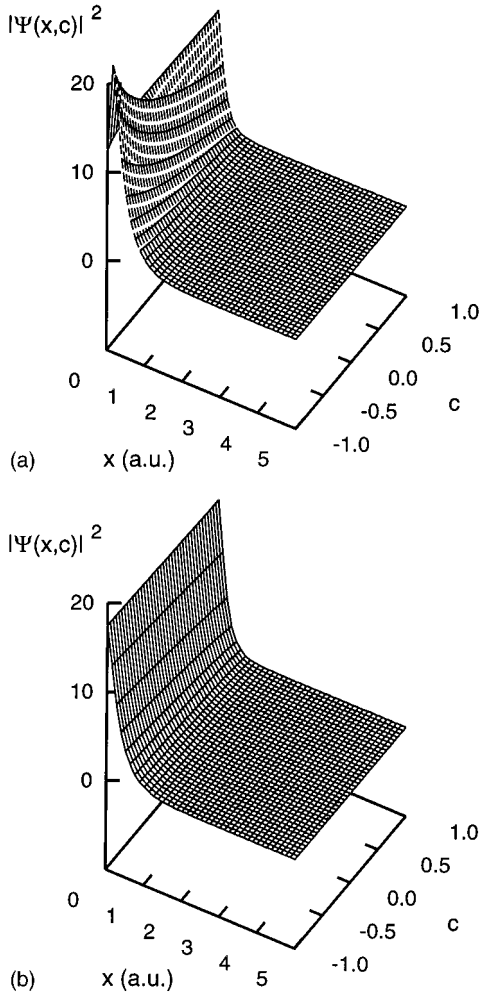

FIG. 4. Modulus square of the wave function for the (0,36) state for (a) standard Jacobi coordinates and (b) our choice, discussed in the text. The function is plotted in arbitrary units. The y coordinate was fixed so that $|\Psi(x=0,y,c=0)|^2$ had a maximum as a function of y.

TABLE II. Energy levels E_{vJ} (a.u.) of the $\overline{p}^4\mathrm{He}^+$ system.

J	$v=0$	$v=1$	$v=2$	$v=3$	$v=4$
30	-3.679769	-3.517965	-3.37509	-3.24887	-3.13731
31	-3.507629	-3.364640	-3.238585	-3.127307	-3.02948
32	-3.353750	-3.227664	-3.116664	-3.019026	-2.933068
33	-3.216235	-3.105370	-3.007965	-2.922430	-2.847329
34	-3.093456	-2.996323	-2.911166	-2.836513	-2.770997
35	-2.984009	-2.899269	-2.825133	-2.760221	-2.703267
36	-2.886669	-2.813102	-2.748847	-2.692612	-2.643233
37	-2.800358	-2.736828	-2.681382	-2.632821	-2.590088
38	-2.724111	-2.669539	-2.621881	-2.580040	-2.543078
39	-2.657045	-2.610391	-2.569536	-2.533514	-2.501511

typical difference for the favored transition wavelengths is less than 0.005 nm.

The accuracy reached in our calculations is not as good as the one in Ref. [22]. On the other hand, it is worth noticing that our numerical scheme is more general. While the variational expansion used by Korobov is mainly suitable only for semiadiabatic three-body systems, our method can be applied to nonadiabatic systems such as the usual helium atom with the same accuracy. Furthermore, calculations of systems in external fields were successfully performed using the present FEM approach [34,36].

IV. RELATIVISTIC CORRECTIONS FOR THE ENERGY LEVELS

Both our nonrelativistic and Korobov's [22] results for the transition wavelengths are about 50 ppm smaller than experimental data. We estimated earlier [23] that relativistic corrections might have an essential influence on the position of the energy levels. In this section we present the relativistic corrections calculated in a systematic way.

First of all, it is worth noticing that the present experimental accuracy [16] makes it meaningful to calculate the relativistic corrections only up to an order of α^2, where α is the fine-structure constant $\alpha=7.29735\times10^{-3}$. These corrections include the following terms [42]: relativistic mass correction terms, Darwin terms for two-particle interactions, spin-orbit force corrections, retardation terms, and an interaction of spin magnetic-dipole moments. Some of these terms include an additional small factor $m_e/m_{\bar{p}}=5.4\times10^{-4}$. In the present calculations we have thus kept only terms of the order $\alpha^2(m_e/m_{\bar{p}})^0$. This means that we have neglected spin-orbit corrections, retardation terms, and corrections due to an interaction of spin magnetic dipoles. Let us now, for consistency, check the relativistic corrections originating in terms from the second and higher equations in system (2). We find that we can neglect a number of terms that are at least of first order in $m_e/m_{\bar{p}}$.

TABLE III. Favored transition wavelengths (nm) of $\overline{p}^4\mathrm{He}^+$.

J	$v=0$	$v=1$	$v=2$	$v=3$	$v=4$
31	264.69	297.17	333.8	374.8	422.5
32	296.10	332.64	373.71	420.79	472.6
33	331.33	372.57	419.17	471.69	531.42
34	371.10	417.83	470.70	530.32	596.91
35	416.30	469.47	529.60	597.22	672.73
36	468.09	528.78	597.27	673.92	758.95
37	527.90	597.36	675.37	762.04	857.35
38	597.57	677.13	765.75	863.26	969.21
39	679.37	770.31	870.45	979.31	1096.14

Thus the only terms to be calculated are the relativistic mass correction term for the electron and Darwin terms for the electron-antiproton and electron-helium interactions. They can be expressed in terms of the electron momentum $\mathbf{p}_e$ and δ functions of the corresponding distances [42]:

$$\Delta E_{vJ}^{(rel)}=\alpha^2\left\langle \psi^{(J0)}\left| -\frac{\mathbf{p}_e^4}{8}+\frac{\pi}{2}[2\,\delta(\mathbf{r}_{23})-\delta(\mathbf{r}_{12})]\right|\psi^{(J0)}\right\rangle. \tag{15}$$

Some care must be taken in the numerical calculation of the mass correction term in Eq. (15). Due the decrease of the bound-state wave function at infinity, we can use a well-known trick [43] and write the first term in Eq. (15) as

$$\begin{aligned}\langle\psi^{(J0)}|\mathbf{p}_e^4|\psi^{(J0)}\rangle&=||\mathbf{p}_e^2\psi^{(J0)}||^2\\&=(2\mu_{23})^2[||(E_{vJ}-V^{Coul})\psi^{(J0)}||^2\\&\quad-2\langle\Delta_x^{(0)}\psi^{(J0)}|\Delta_y^{(0)}\psi^{(J0)}\rangle-||\Delta_y^{(0)}\psi^{(J0)}||^2].\end{aligned} \tag{16}$$

In Fig. 5 we show contributions of the two terms in Eq. (15) to the total-energy corrections as a function of J for $v=2$. One notices a big cancellation effect: the final correction is about 5 times smaller than each term. There is an even bigger cancellation effect for the transition wavelengths because the difference $\Delta E_{vJ}^{(rel)}-\Delta E_{vJ-1}^{(rel)}$ is about 10 times smaller than each correction. Notice also that the resulting cancellation effect in $\overline{p}\mathrm{He}^+$ is a few times smaller than in the usual helium atom [42] and in this sense the relativistic effects manifest themselves more strongly in the antiprotonic helium.

The calculated results for $\Delta E_{vJ}^{(rel)}$ are presented in Table IV. As the values of the relativistic corrections are rather small, they can be calculated with a smaller relative accuracy than the nonrelativistic energies. On the other hand, it was

TABLE IV. Relativistic corrections $\Delta E_{vJ}^{(rel)}$ (10^{-6} a.u.) for the $\overline{p}^4\mathrm{He}^+$ system.

J	$v=0$	$v=1$	$v=2$	$v=3$	$v=4$
30	-28.70	-32.94	-37.26	-41.59	-48.58
31	-31.61	-36.27	-40.97	-45.68	-52.39
32	-34.80	-39.84	-44.87	-49.86	-56.32
33	-38.27	-43.64	-48.96	-54.12	-60.31
34	-42.03	-47.67	-53.19	-58.45	-64.33
35	-46.08	-51.92	-57.53	-62.79	-68.31
36	-50.40	-56.36	-61.94	-67.08	-72.20
37	-54.98	-60.93	-66.37	-71.27	-75.94
38	-59.77	-65.59	-70.77	-75.52	-79.47
39	-64.72	-70.25	-75.04	-79.28	-82.76

demonstrated [28,29] that the FEM gave fewer errors in the wave-function matrix elements than the global basis set method when the same accuracy for eigenvalues was reached. Thus we estimate the accuracy of the present relativistic corrections to be about 10^{-7} a.u. using our wave functions. Since Korobov's nonrelativistic energy levels are more accurate than ours, we mean that we will obtain better estimates of the exact total energies by using his nonrelativistic energies and our relativistic corrections.

Because of the big cancellation effect demonstrated above, the correction of the next order with respect to α could have an essential influence on the energy-level corrections. The main additional correction arises from the Lamb shift, which is of order $\alpha^3\ln(1/\alpha)$ [42]. It is known [42,44] that the Lamb shift for one electron in a heliumlike atom with a nuclear charge Z can be expressed as

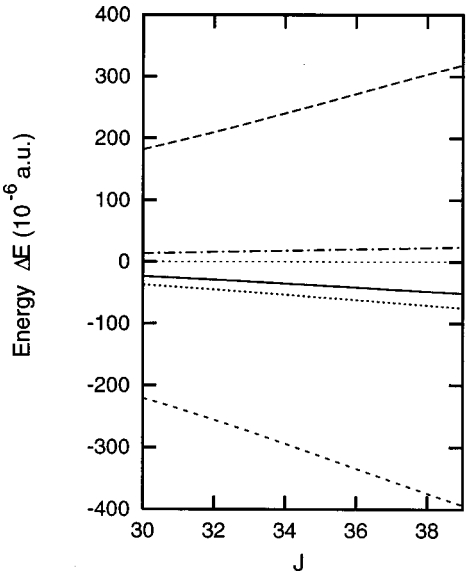

FIG. 5. Relativistic corrections for $(2,J)$ states. The dashed line, short-dashed line, and dotted line correspond to Darwin terms, the relativistic mass correction term, and $\Delta E_{2J}^{(rel)}$, respectively. The dash-dotted line corresponds to the Lamb shift ΔE_{2J}^{L} and the solid line to the total (relativistic and QED) correction.

TABLE V. Lamb shift ΔE_{vJ}^{L} (10^{-6} a.u.) for the $\overline{p}^4\mathrm{He}^+$ system.

J	$v=0$	$v=1$	$v=2$	$v=3$	$v=4$
30	11.6	12.9	13.5	15.6	17.0
31	12.5	13.8	15.2	16.2	18.1
32	13.4	14.8	16.3	17.7	19.1
33	14.4	15.9	17.3	18.8	20.2
34	15.4	16.9	18.4	19.9	21.2
35	16.5	18.1	19.6	21.0	22.3
36	17.7	19.2	20.7	22.1	23.3
37	18.9	20.4	21.8	23.1	24.2
38	20.2	21.6	23.0	24.1	25.1
39	21.4	22.8	24.1	25.1	26.0

$$\Delta E_{vJ}^{L}=\frac{8\alpha^3 Z}{3}\langle\psi^{(J0)}|\,\delta(\mathbf{r}_{23})\,|\psi^{(J0)}\rangle \times\left(\frac{19}{30}+2\ln\frac{1}{\alpha Z}-\ln\frac{K_0}{Z^2\ \mathrm{Ry}}\right). \tag{17}$$

Here K_0 is the Bethe average excitation energy. An expression similar to Eq. (17) could be written for the electron-antiproton interaction. However, we neglect this additional term as the calculation shows that $\langle\delta(\mathbf{r}_{12})\rangle\leqslant\frac{1}{10}\langle\delta(\mathbf{r}_{23})\rangle$ for all levels. Furthermore, the expression for the electron-antiproton Lamb shift is half of this value since $Z=1$ here. Thus we can estimate that $\Delta E_{vJ}^{L}(e\overline{p})\leqslant 0.05\Delta E_{vJ}^{L}(e\mathrm{He}^{2+})$. The next uncertainty arises from K_0. We have adopted $K_0=84$ Ry as for the usual He atom [42] despite the fact that this value must be smaller due to the screening-charge effect in our system. The total error introduced in this way can be estimated to be less than 5% of ΔE_{vJ}^{L} and is produced mainly by the neglected electron-antiproton term.

The values of ΔE_{vJ}^{L} are presented in Table V and illustrated for $(2,J)$ states in Fig. 5. One can see that these values are not small in comparison with relativistic corrections and constitute about $\frac{1}{3}$ of $\Delta E_{vJ}^{(rel)}$. Thus both relativistic and QED corrections must be taken into account in order to obtain a precise consistent comparison between theoretical and experimental data.

In Table VI we present the experimentally known transition wavelengths, Korobov's and our nonrelativistic results, as well as relativistically corrected values. Because there were no details of calculations in Refs. [16,22], we cannot now analyze the existing small differences of relativistic corrections. When $\Delta E_{vJ}^{(rel)}$ are used only for the corrections, we have very good agreement with present experimental data. However, our final transition wavelengths, including both relativistic $\Delta E_{vJ}^{(rel)}$ and Lamb shift ΔE_{vJ}^{L} corrections, are in all cases shorter than the experimentally measured ones. It is worth noticing that in a very recent paper [15] there was reported a slow dependence of the measured wavelength on the pressure of a helium gas target: 529.621 nm at 1.0 bar and 529.623 nm at 1.3 bar. It was stated that other known wavelengths had a similar dependence. (They were measured at 0.6–1.0 bar [7,11,16].) As our values are calculated for the isolated system, they have to be compared with experimental

TABLE VI. Comparison between theoretical and experimental favored transition wavelengths (nm): $(v,J)\rightarrow(v,J-1)$. Our results are presented when relativistic corrections $\Delta E_{vJ}^{(rel)}$ only and both relativistic $\Delta E_{vJ}^{(rel)}$ and Lamb shift ΔE_{vJ}^{L} corrections are taken into account.

	Nonrelativistic			Relativistic		
(v,J)	Present	Ref. [22]	Refs. [16,22]	$\Delta E_{vJ}^{(rel)}$	$\Delta E_{vJ}^{(rel)}+\Delta E_{vJ}^{L}$	Experiment
(2,34)	470.702	470.7051	470.7241	470.7257	470.720	470.724(2)[a]
(3,35)	597.224	597.2287	597.2563	597.2627	597.254	597.259(2)[b]
(2,36)	597.266	597.2634	597.298	597.2979	597.289	597.298(2)[c]
(1,37)	597.363	597.3626	597.398	597.3984	597.389	597.397(2)[c]
(0,38)	597.575	597.5716	597.609	597.6092	597.601	597.607(2)[c]
(2,35)	529.600	529.5964	529.623	529.6231	529.616	529.622(3)[d,c]
(1,36)	528.778	528.7810	528.808	528.8082	528.801	528.808(8)[c]
(0,37)	527.900	527.9032	527.931	527.9312	527.924	527.930(2)[c]

[a]Reference [11].
[b]Reference [7].
[c]Reference [16].
[d]Reference [15].

data extrapolated to the zero pressure. The processes behind the above-mentioned pressure dependence are rather complicated. However, if we just linearly extrapolated the recent experimental wavelength measurements [15] to zero pressure, we obtain 529.614 nm, which is in excellent agreement with our theoretical result.

V. TRANSITION PROBABILITIES

In the previous sections we have calculated the energy levels for the $\overline{p}^4\mathrm{He}^+$ system that are in a quite good agreement with experimental data. In order to compare with experiment, however, we need to show that the intensity of the measured [8,11] and calculated transitions are comparable.

The lifetime of the state (v,J) associated with radiative transitions to all lower states is

$$\tau_{vJ}=\left(\sum_{E_{v'J'}<E_{vJ}} A_{vJ,v'J'}\right)^{-1}, \tag{18}$$

where the Einstein coefficient $A_{vJ,v'J'}$ can be expressed in terms of the oscillator strength $f_{vJ,v'J'}$ by the relation

$$A_{vJ,v'J'}=-2\alpha^3(E_{vJ}-E_{v'J'})^2 f_{vJ,v'J'}. \tag{19}$$

The oscillator strengths have been calculated in terms of the wave-function components $\psi^{(Js)}(x,y,c)$. The calculation is cumbersome but straightforward. We obtain

$$f_{vJ,v'J'}=-\frac{2}{3}(E_{vJ}-E_{v'J'})\delta_{J',J\pm1}\frac{J_>}{2J+1}\times\left|\sum_{s=0}^{J}\langle\psi^{(Js)}|D|\psi^{(J's)}\rangle\right|^2, \tag{20}$$

where $J_>=\max\{J,J'\}$ and the dipole operator element

$$D=y+\left(1+\frac{m_2}{m_2+m_3}\right)xc. \tag{21}$$

In Eq. (20) we assume that the wave function is normalized such that

$$\sum_{s=0}^{J}||\psi^{(Js)}(x,y,c)||^2=1. \tag{22}$$

If only the zero component $\psi^{(J0)}$ is involved in the calculation, Eq. (20) resembles the expression used by Shimamura [17] for the calculation of the transition probabilities in the BO approximation. The validity of this approximation will be discussed below.

The lifetimes for states with the vibrational quantum numbers $v=0,1,2$ are presented in Fig. 6. Both the results using the three-equation formalism and the one-equation formalism are displayed. Despite the fact that the wave function for

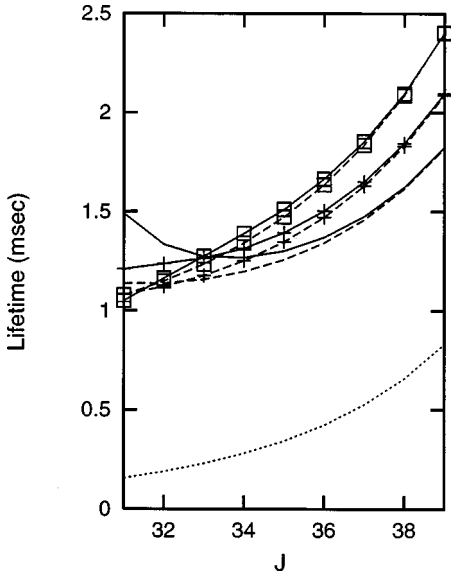

FIG. 6. Radiative lifetimes τ_{vJ}. The lines without symbols, with crosses, and with squares correspond to $v=0,1,2$, respectively. The solid line corresponds to the calculations with three equations and the dashed one refers to a one-equation calculation. The dotted line represents a calculation without the core-polarization effect.

one equation does not coincide with the BO function, they are similar since both include atomic-core polarization effects while both of them do not include electronic excitations. The displayed lifetimes coincide in general with the results in Ref. [19]. However, a detailed comparison reveals some differences. For $v=0$ both the present and previous [19] calculations give lifetimes that are decreasing with J in the range $J=30$–34. While the previous paper [19] reports a similar behavior for $v=1$, we find a slow, smooth increase of τ in the entire investigated range for both $v=1$ and 2. One can see that for larger values of momentum ($J\geqslant 34$–35) the influence of the next equations is weak and becomes much smaller with increasing J. However, for smaller J this influence changes the lifetime considerably, especially for higher values of v.

Actually, this change is defined only by the first term $s=0$ in Eq. (20), while other terms are negligibly small. This means that the reason is only a change of the component $\psi^{(J0)}$ in the few-equation calculations. This may be understood as follows. It is known that the core-polarization effect is rather big and the lifetime changes drastically when one takes this effect into account [19]. To illustrate this effect, in Fig. 6 we show the lifetimes calculated without core-polarization effect, i.e., for $D=y$. Only the P-wave component of the wave function contributes to the core-polarization effect, while the S component mainly defines the energy values. Thus even small changes in the wave function can influence the lifetime considerably when they refer to the P component. In our calculations we have exactly such a situation because one can in Eq. (2) see that the off-diagonal terms connecting $\psi^{(J0)}$ and $\psi^{(J1)}$ are exactly zero for the S component of the total wave function. Thus, while both $\psi^{(J1)}$ and the P component of $\psi^{(J0)}$ are small, their interaction can produce considerable changes in lifetimes in spite of the fact that the energy shift due to $\psi^{(J1)}$ is rather small.

The same situation can be observed for the Einstein coefficients presented in Fig. 7. One can see that the lifetimes for $J\geqslant 34$ are essentially described by the favored transitions, $\Delta v=0$, $\Delta J=-1$. The next Einstein coefficients for the transitions $\Delta v=-1$, $\Delta J=-1$ are smaller ($\leqslant 15\%$) and decrease the lifetimes only slightly. The analysis of the propensity rules given in Ref. [17] is thus valid for these values of J.

Also, the variation of τ for $(0,J)$ initial states are small for arbitrary values of J. This is because the only possible transitions are favored transitions ($\Delta v=0$) and transitions with $\Delta v=+1$. The Einstein coefficients for the latter ones are small due to small energy differences in Eq. (19).

On the other hand, the changes in the Einstein coefficients with the number of equations for larger v and smaller J can be essential. Furthermore, nonfavored transitions can become comparable with favored ones. The reason for such drastic changes is the same as that pointed out above, namely, that a strong coupling of two small components defines a large part of the dipole matrix element in Eq. (20). However, these Einstein coefficients are of academic interest only. The states with values $J\leqslant 33$ and $v\geqslant 2$ are unstable with respect to Auger decays [6] and their lifetimes are in practice defined by Auger processes while the radiative decay rates are smaller by a few orders of magnitude [6]. This

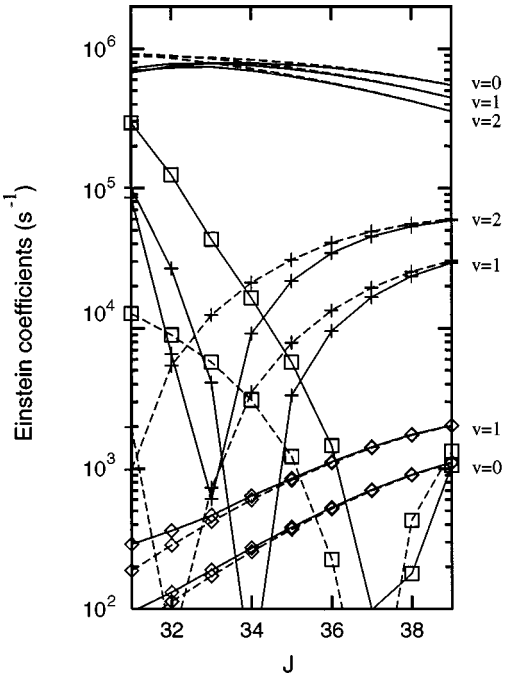

FIG. 7. Einstein coefficients $A_{vJ,v'J'}$. The solid line corresponds to the calculations with three equations and the dashed one refers to a one-equation calculation. The lines without symbols, with crosses, and with diamonds correspond to the $(v,J)\rightarrow(v,J-1)$, $(v,J)\rightarrow(v-1,J-1)$, and $(v,J)\rightarrow(v+1,J-1)$ transitions, respectively. The lines with squares refer to the $(2,J)\rightarrow(0,J-1)$ transition.

implies that we are not able to describe these states as bound states. Taking into account the resonant properties of these states may lead to considerable changes in the corresponding wave functions, energy eigenvalues [45], and therefore radiative lifetimes.

Finally, we compare known experimental [8,11] and theoretical values of the decay rates. They are represented in Table VII. One can see that various theoretical results agree with each other rather well and depend only slightly on the method of calculations. However, despite satisfactory agreement with experimental data for $(3,35)\rightarrow(3,34)$ transition, the difference in the decay rates for the $(2,34)\rightarrow(2,33)$ transition is rather large. This may be explained by the fact that one has neglected Auger decays in all of the theoretical calculations. Thus, as pointed out above, taking into account Auger processes is in principle necessary for an accurate description of any processes in the $\bar{p}\mathrm{He}^+$ system.

TABLE VII. Experimental and theoretical decay rates (10^6 s^{-1}) for two states of $\bar{p}$-^{4}He$^+$.

Source \ State	(2,34)	(3,35)
[17]	0.754	0.619
[6]	0.734	0.614
[21]	0.713	0.597
present work	0.722	0.599
experiment	1.18(4)[a]	0.72(2)[b]

[a]Reference [11].
[b]Reference [8].

VI. CONCLUSION

In this paper we present a recently developed extension to a three-dimensional finite-element code. Earlier, the implemented method manifested itself as a convenient tool for studies of various quantum-mechanical problems: above threshold ionization of hydrogen [34], $td\mu$ and $dd\mu$ muonic molecular ions [35], and laser-induced recombination to excited states of hydrogenlike ions [36]. Using the total angular momentum representation, we have been able to calculate here energy levels and wave functions for the antiprotonic helium system with rather high accuracy.

Relativistic and QED corrections to the energy levels in the main order in α were calculated in terms of matrix elements of the nonrelativistic wave functions. Excellent agreement was reached between our theoretical results and experimental data. However, in spite of this agreement, calculated and measured data for decay rates differ considerably. The reason for this discrepancy is a neglect of resonant properties of the involved states. Thus precise calculations of Auger processes should be performed in order to obtain the detailed description of the dynamics of the antiprotonic helium. Such a study could be especially interesting for the $\overline{p}^3\mathrm{He}^+$ system in connection with recently observed intermediate (between Auger and radiative) lived states [13]. We believe that the recently calculated high-precision wave functions and energy levels for the $\overline{p}\mathrm{He}^+$ system will be useful for the further investigation of this interesting and intensively studied system.

ACKNOWLEDGMENTS

We would like to thank Professor T. Yamazaki for valuable information about the current stages of the antiproton helium project at CERN, Dr. E. Lindroth for discussions about the relativistic corrections, and Dr. A. Scrinzi for support during the early stage of the project. This work was supported by generous grants from the Royal Swedish Academy of Sciences and the Wenner-Gren Center Foundation.

[1] G. T. Condo, Phys. Lett. **9**, 65 (1964).
[2] J. E. Russel, Phys. Rev. A **1**, 721 (1970); **1**, 735 (1970); **1**, 742 (1970).
[3] R. Ahlrichs, O. Dumbrajs, H. Pilkuhn, and H. G. Schaile, Z. Phys. A **306**, 297 (1982).
[4] M. Iwasaki *et al.*, Phys. Rev. Lett. **67**, 1246 (1991).
[5] T. Yamazaki *et al.*, Nature (London) **361**, 238 (1993).
[6] N. Morita, K. Ohtsuki, and T. Yamazaki, Nucl. Instrum. Methods Phys. Res. A **330**, 439 (1993).
[7] N. Morita *et al.*, Phys. Rev. Lett. **72**, 1180 (1994).
[8] R. S. Hayano *et al.*, Phys. Rev. Lett. **73**, 1485 (1994); **73**, 3181 (1994).
[9] S. N. Nakamura *et al.*, Phys. Rev. A , **49**, 4457 (1994).
[10] E. Widmann *et al.*, Phys. Rev. A **51**, 2870 (1995).
[11] F. E. Maas *et al.*, Phys. Rev. A **52**, 4266 (1995).
[12] H. A. Torii *et al.*, Phys. Rev. A **53**, R1931 (1996).
[13] B. Ketzer *et al.*, Phys. Rev. A **53**, 2108 (1996).
[14] E. Widmann *et al.*, Phys. Rev. A **53**, 3129 (1996).
[15] R. S. Hayano *et al.*, Phys. Rev. A **55**, R1 (1997).
[16] B. Ketzer *et al.*, Phys. Rev. Lett. **78**, 1671 (1997).
[17] I. Shimamura, Phys. Rev. A **46**, 3776 (1992).
[18] I. V. Puzynin, T. P. Puzynina, S. I. Vinitsky, and V. I. Puzynin, Hyperfine Interact. **101/102**, 493 (1996).
[19] T. Yamazaki and K. Ohtsuki, Phys. Rev. A **45**, 7782 (1992).
[20] P. T. Greenland and R. Thurwachter, Hyperfine Interact. **76**, 355 (1993).
[21] O. I. Kartavtsev, Phys. At. Nucl. **59**, 1483 (1996).
[22] V. I. Korobov, Phys. Rev. A **54**, R1749 (1996); Hyperfine Interact. **101/102**, 479 (1996).
[23] E. Yarevsky and N. Elander, Europhys. Lett. **37**, 453 (1997).
[24] W. A. Beck, L. Wilets, and M. A. Alberg, Phys. Rev. A **48**, 2779 (1993).
[25] G. Ya. Korenman, Phys. At. Nuclei **59**, 1665 (1996); Hyperfine Interact. **101/102**, 463 (1996).
[26] K. W. Morton, Comput. Phys. Rep. **6**, 1 (1987).
[27] C. Bottcher, Adv. At. Mol. Phys. **20**, 241 (1985).
[28] F. S. Levin and J. Shertzer, Phys. Rev. A **32**, 3285 (1985); J. Shertzer and F. S. Levin, *ibid.* **43**, 2531 (1991).
[29] J. Ackermann and J. Shertzer, Phys. Rev. A **54**, 365 (1996).
[30] D. Heinemann, B. Fricke, and D. Kolb, Phys. Rev. A **38**, 4994 (1988).
[31] J. Olsen, P. Jorgensen, and J. Simons, Chem. Phys. Lett. **169**, 463 (1990).
[32] D. Sundholm and J. Olsen, Chem. Phys. Lett. **171**, 53 (1990).
[33] A. Scrinzi and N. Elander, J. Chem. Phys. **98**, 3866 (1993).
[34] A. Scrinzi, N. Elander, and B. Piraux, Phys. Rev. A **48**, R2527 (1993).
[35] A. Scrinzi, Comput. Phys. Commun. **86**, 67 (1995).
[36] A. Scrinzi, N. Elander, and A. Wolf, Z. Phys. D **34**, 185 (1995).
[37] D. A. Varshalovish, A. M. Moskalev, and V. K. Khersonskii, *Quantum Theory of Angular Momentum* (World Scientific, Singapore, 1989).
[38] C. F. Curtiss, J. O. Hirschfelder, and F. T. Adler, J. Chem. Phys. **18**, 1638 (1950).
[39] W. H. Press, B. P. Flannery, S. A. Teukolsky, and W. T. Vetterling, *Numerical Recipes* (Cambridge University Press, Cambridge, 1989).
[40] Particle Data Group, Phys. Lett. B **239**, 1 (1990).
[41] E. Balslev and J. M. Combes, Commun. Math. Phys. **22**, 280 (1971); B. Simon, Ann. Math. **97**, 247 (1973); C. Van Winter, J. Math. Anal. Appl. **47**, 633 (1974); several papers in *Resonances*, edited by E. Brändas and N. Elander, Lecture Notes in Physics Vol. 325 (Springer, Berlin, 1989).
[42] H. A. Bethe and E. E. Salpeter, *Quantum Mechanics of One- and Two-Electron Atoms* (Plenum, New York, 1977).
[43] C. L. Pekeris, Phys. Rev. **112**, 1649 (1958).
[44] A. Kono and S. Hattori, Phys. Rev. A **34**, 1727 (1986).
[45] E. Brändas, N. Elander, and P. Froelich, Int. J. Quantum Chem. **98**, 443 (1978).